УДК 537.591.15

Lagutin A. A., Plyasheshnikov A. V., Melentjeva V. V., Misaki A., Raikin R. I.

Lateral distribution of electrons in air showers[1]

We report on the results obtained for the lateral distribution of electrons in both the electromagnetic cascade in the air and the extensive air shower for the primary energies up to 10^9 GeV.

We have found a new scaling property of the lateral distribution of electrons in pure electromagnetic cascade and give a parametrization on the invariant part of the lateral distribution function up to 3000 m from the core location.

We have carried out the Monte Carlo simulation of the extensive air shower, based on the quark-gluon strings model for hadron-nucleous interactions with the use of this parametrization. The results show that the lateral distribution function in the extensive air shower keeps the same invariant part as the one in pure electromagnetic cascade. Besides this phenomenon is poorly sensitive to the change of the basic parameters of interactions model.

Introduction

One of the basic characteristics of the extensive air shower (EAS) development is the lateral distribution function (LDF) of the electrons. Estimates on the shower size, the core position and the age parameter are made by using LDF. Knowledge of the correct LDF is therefore of great importance in EAS research.

The lateral distribution function of the EAS electrons is usually obtained as a result of a parametrization of the lateral distribution of charged particles in the pure electromagnetic cascade (EMC). The well-known Nishimura-Kamata-Greisen (NKG) function [1] has been used as a lateral distribution function of the total electron number for many years. However, during 1975–1979 some works [2–6] appeared which questioned the applicability of the NKG results. For example, detailed Monte Carlo calculations of the LDF for cascades generated by 10 and 10^2 GeV photons [5] and our calculatons [6] for the primary energies $E_\gamma = (10 \div 10^6)$ GeV and $r \leq 200$ m gave much narrower distribution than the NKG formula did.

In [7] the LDF have been investigated for the distances from the shower core up to 500 m. At the same time the design studies for new air shower arrays (Auger Project, EAS–1000 etc.) require detailed description of the lateral shower development at least up to $r \approx 2000$ m in the cascades generated by $10^7 \div 10^{10}$ GeV photons. Our calculations performed in [8-13] were specifically carried out for the study on the lateral shower development in the radial distance range $r \approx (1 \div 3000)$ m. Two dif-

ferent approaches for these calculations were applied to get the lateral distribution function data: the semi-analytical Monte Carlo method and the method based on the numerical solution of adjoint cascade equations.

In this paper we report on the results obtained for the electron lateral distribution of the EMC generated by $10 \div 10^9$ GeV photons in a wide range of distances from the shower axis. We have found a new scaling property of the electron lateral distribution function of the EMC generated by $10 \div 10^9$ GeV photons in a wide range of distances from the shower core. We give a parametrization of the invariant part of the LDF. Using this parametrization we have made the Monte Carlo calculations for the lateral distribution of extensive air shower for the primary proton energies $E_p = 10^5 \div 10^9$ GeV in the real (inhomogenious) atmosphere at the different observation levels. The scaling property of the LDF in the extensive air shower and its sensitivity to the change of the parameters of interactions model has been investigated.

The results presented in this paper enable to solve the problems appearing in the design studies for new large air-shower arrays and interpretation of the observational data.

1. Calculation methods in the case of the pure electromagnetic cascade

Two different approaches are used to calculate the LDF of the electrons in electromagnetic cascade: the semi-analytical Monte Carlo (SAMC) method and the method based on the numerical solution of adjoint cascade equations. Below we give a brief overview of these approaches.

SAMC method

To reduce the computational time a special approach—the semi-analytical Monte Carlo method—is applied by us to perform simulations (for its detailed description see publications [7,14, 15]). Our SAMC method gives a possibility of nice account for the multidimensional structure of the cascade and properties of the detectors. At the same time this approach provides a weak (logarithmic) growth of the computational time with the primary energy.

In our SAMC method the high energy part of electromagnetic cascade above approximately 10 GeV is considered as an "imaginary source" of low energy particles (all other cascade particles). The complete Monte Carlo method is applied to simulate the propagation of low energy particles. The phase coordinates of generation points of such particles (the space coordinates, the emission angles, the energy, etc.) are randomly selected in accordance with the multidimensional density of the "imaginary source". A special kind of adjoint cascade equations is derived for the differential density of this source. In the high energy region a number of approximations (neglection by the ionization losses and the Compton scattering, the small angle treatment of the multiple scattering of electrons, neglection by the lateral displacement of cascade particles etc.) can be used giving a possibility to solve equations for the differential density of the "imaginary source" by standard analytical methods.

The code of the complete Monte Carlo method used for the simulations in the SAMC approach was developed in the Altai State University (see for details [7]). In comparison to other simulation codes (for example, EGS, MOCCA) essentially more precise probability distributions are applied here to simulate the multiple scattering of cascade charged particles. Adoption of these probability distributions gives a possibility to increase considerably the length of multiple scattering segments into which the trajectory of a charged particle is divided in the process of simulation. The latter consumes sufficiently the computational time.

Numerical solution of adjoint equations

Consider a point detector measuring the integrated over angles flux of electrons with the energies higher than a threshold value E_{th} and assume that it is placed in the infinite homogeneous medium. The primary particle with the energy E generating the shower is located at the distance t from the detector. According to the evident symmetry the reading of such a detector depends, except for the energies E and E_{th}, on t and the angle θ between the primary particle movement direction and the direction towards the detector. Let us mark the mean value of detector readings by $N_e(t, \theta, E)$ and $N_\gamma(t, \theta, E)$ in the case of the primary electron and photon, respectively. Since the high energy particle penetration is dominated by the small-angle scattering, the small angle approximation can be used. In this approximation the functions N_e, N_γ satisfy the adjoint equations which have the form:

$$\left[\frac{\partial}{\partial t} - \frac{\theta}{t} \frac{\partial}{\partial \theta} + \sigma_e(E) \right] N_e(t, \theta, E) =$$

$$= \int_{E_{th}}^{E} dE' W_{ee}(E \to E') N_e(t, \theta, E') +$$

$$+ \int_{E_{th}}^{E} dE' W_{e\gamma}(E \to E') N_\gamma(t, \theta, E') -$$

$$- \int_{0}^{2\pi} d\phi \int_{0}^{\infty} W_s(E, \Theta)[N_e(t, \theta, E) -$$

$$- N_e(t, \theta', E)]\theta' d\theta', \quad (1)$$

$$\left[\frac{\partial}{\partial t} - \frac{\theta}{t} \frac{\partial}{\partial \theta} + \sigma_\gamma(E) \right] N_\gamma(t, \theta, E) =$$

$$= \int_{E_{th}}^{E} dE' W_{\gamma e}(E \to E') N_e(t, \theta, E') +$$

$$+ \int_{E_{th}}^{E} dE' W_{\gamma\gamma}(E \to E') N_\gamma(t, \theta, E'), \quad (2)$$

where $W_s(E, \Theta)$ is the differential cross-section of Coulomb scattering to the angle $\Theta = \sqrt{\theta^2 + \theta'^2 - 2\theta\theta' \cos\phi}$, $t = z^* - z$ is the distance between the primary particle and the plane, where boundary conditions are defined. Boundary conditions for N_e and N_γ have the form:

$$\lim_{t \to 0} 2\pi t^2 N_e(t, \theta, E) = \begin{cases} \delta(\theta)/\theta, & E \geq E_{th}, \\ 0, & E < E_{th}, \end{cases}$$

$$\lim_{t \to 0} 2\pi t^2 N_\gamma(t, \theta, E) = 0.$$

Note that in the small angle approximation the variable t can be interpreted as the distance from the primary particle along its movement direction to the observation plane which is perpendicular to this direction. The radius r of the observation point in this plane is expressed through θ by the relation

$r = \theta t$. The normalized lateral distribution function can be expressed as

$$f(r, t, E) = \frac{N(t, r/t, E)}{2\pi t^2 \displaystyle\int\limits_0^\infty d\theta\, \theta\, N(t, \theta, E)}.$$

The numerical method of solution of equations (1),(2) developed in [16] consists of the following steps.

a) The Fourier-Bessel transformation is performed with respect to the variable θ. As the result one can obtain, instead of (1),(2), the following expressions:

$$\left[\frac{\partial}{\partial t} + \sigma_e(E) + A(E, q)\right] N_e(t, q, E) =$$

$$= \int\limits_{E_{\mathrm{th}}}^E dE' W_{ee}(E \to E') N_e(t, q, E') +$$

$$+ \int\limits_{E_{\mathrm{th}}}^E dE' W_{e\gamma}(E \to E') N_\gamma(t, q, E'); \quad (3)$$

$$\left[\frac{\partial}{\partial t} + \sigma_\gamma(E)\right] N_\gamma(t, q, E) =$$

$$= \int\limits_{E_{\mathrm{th}}}^E dE' W_{\gamma e}(E \to E') N_e(t, q, E') +$$

$$+ \int\limits_{E_{\mathrm{th}th}}^E dE' W_{\gamma\gamma}(E \to E') N_\gamma(t, q, E'), \quad (4)$$

$$N_e(t = 0, q, E) = \begin{cases} 1, & E \geq E_{\mathrm{th}}, \\ 0, & E < E_{\mathrm{th}}, \end{cases}$$

$$N_\gamma(t = 0, q, E) = 0, \quad (5)$$

$$N_\alpha(t, q, E) = 2\pi t^2 \int\limits_0^\infty N_\alpha(t, \theta, E) J_0(tq\theta)\theta d\theta,$$

$$\alpha = e, \gamma;$$

$$A(E, q) = 2\pi \int\limits_0^\infty W_s(E, \theta)[1 - J_0(q\theta)]\theta d\theta. \quad (6)$$

b) The primary energy range $(E_{\mathrm{th}}, E_{\mathrm{max}})$ is divided into small segments in the logarithmically constant scale. In each of these segments the energy dependence of functions N_e, N_γ is approximated by the Lagrange polynomial of a certain power (the third power in our analysis).

As a result of this operation we will obtain a system of the ordinary differential equations for the Lagrange polynomial coefficients. It can be easily integrated over depth t.

c) The procedure described in b) is carried out for a set of the values of transformation parameter q. After that we can perform the inverse transformation by the numerical way

$$N_\alpha(t, \theta, E) = \frac{1}{2\pi t^2} \int\limits_0^\infty N_\alpha(t, q, E) J_0(tq\theta) q dq,$$

$$\alpha = e, \gamma,$$

and obtain quantities N_e, N_γ for the necessary values of t, θ and E. In papers [7,17] it was noted that in the range $r \geq 200$ m the deflection of cascade photons in the Compton scattering process essentially influences on the shape of the LDF. In this connection we developed a special approximate technique to take into account the Compton scattering angle. This technique leads to a slight modification of adjoint equations (1)–(4). It is described in details in [8].

2. The lateral distribution of electrons in the electromagnetic cascade

The case of the homogeneous atmosphere

We start with the calculational data obtained for the homogeneous atmosphere (density $\rho_0 = 1.22 \cdot 10^{-3}\mathrm{g/cm}^3, t_0 = 296$ m). The results correspond to the primary photon energies $E_\gamma = (10 \div 10^9)$ GeV and the cascade age parameters $s \approx (0.6 \div 1.6)$ derived from equation $t = -(\ln E_\gamma/\beta) \,/\, \lambda_1'(s)$, where $\beta = 80$ MeV. The threshold energy E_{th} was chosen to be equal to 0.1 MeV. According to [6] $E_{\mathrm{th}} = 0.1$ MeV can be regarded as the almost same as $E_{\mathrm{th}} = 0$, which corresponds to E_{th} in the total number of electrons. The examples of the LDF for three values of the cascade age parameters $(s = 0.6; 1.0; 1.4)$ and energies $E = 10^2, 10^7$ GeV are shown in Fig. 1.

To analyse the dependence of the LDF on the energy E_γ and cascade age s, we use the variable $x = r/r_{\mathrm{m.s.r.}}$ [18], where $r_{\mathrm{m.s.r.}}(E, s)$ is the mean square radius of the shower

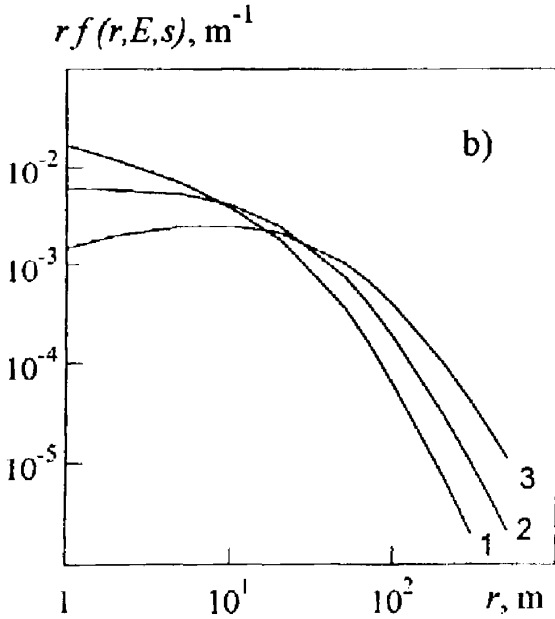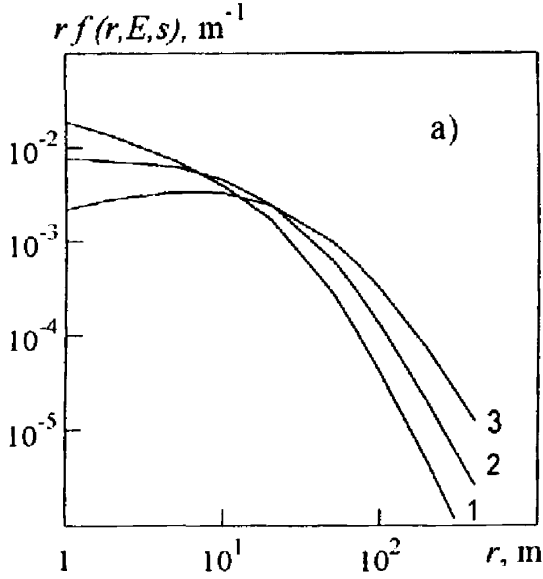$$r_{\mathrm{m.s.r.}}(E, s) = \left[2\pi \int\limits_0^\infty r^2 f(r, E, s) r\, dr\right]^{1/2}. \quad (7)$$

Figure 1. The lateral distribution functions for the cascade ages $s = 0.6$ (1), 1.0 (2), 1.4 (3) and for primary photon energies $E_\gamma = 10^2 (a), 10^7 (b)$ GeV.

Table 1

Data on the $r = x r_{\mathrm{m.s.r.}}$(m) for minimum and maximum values of x considered in our paper. $E_\gamma = 10^8$ GeV

x	s
	0.6	0.8	1.0	1.2	1.4
0.05	1.7	2.4	3.5	5.2	7.7
25	830	1210	1770	2600	3860

The lateral distribution $f(x, E, s)$ with respect to x is related with $f(r, E, s)$ by the formula

$$x f(x, E, s) = r_{\mathrm{m.s.r.}} r f(r, E, s). \tag{8}$$

This distribution function is normalized as

$$2\pi \int\limits_0^\infty x f(x, E, s) \, dx = 1. \tag{9}$$

Detailed analysis of the calculational data in [11] allows us to conclude that distribution $x f(x, E, s)$ as a function of the variable x in the region $0.05 \leq x \leq 25$ does not depend practically on the primary energy E and the shower age parameter s:

$$x f(x, E, s) \approx x f(x). \tag{10}$$

This new scaling property on the lateral distribution is illustrated in Fig. 2. We approximate $x f(x)$ as

$$
x f(x) = \exp\{-3.63 - 1.89 \ln x - \\
- 0.370 \ln^2 x - 0.0168 \ln^3 x\}. \tag{11}
$$

Our fitting function is also shown in Fig. 2. In Table 1 we present the range of variation of r corresponding to the region $0.05 \leq x \leq 25$.

Thus, the electron lateral distribution $r f(r, E, s)$ in the radial region $x \geq 0.05$ is well described by the formula

$$r f(r, E, s) = \frac{x f(x)}{r_{\mathrm{m.s.r.}}(E, s)},$$

where $x f(x)$ is given by (11) and

$$
r_{\mathrm{m.s.r.}}(E, s) = 296 \exp\{-3.69 + 0.0505 \ln E - \\
- 0.00175 \ln^2 E + s \, [1.81 + 0.00638 \ln E - \\
- 0.0826 / \ln E]\}, \mathrm{m},
$$

for $s = (0.5 \div 1.6)$ and $E_\gamma = (10 \div 10^9)$ GeV. The electron density Δ can be calculated from the function $f(r, E, s)$ by $\Delta = N(t, E) f(r, E, s)$, where $N(t, E)$ is the total number of electrons at the observation level in photon-initiated cascade. The results of our calculations of $N(t, E, s)$ with the use
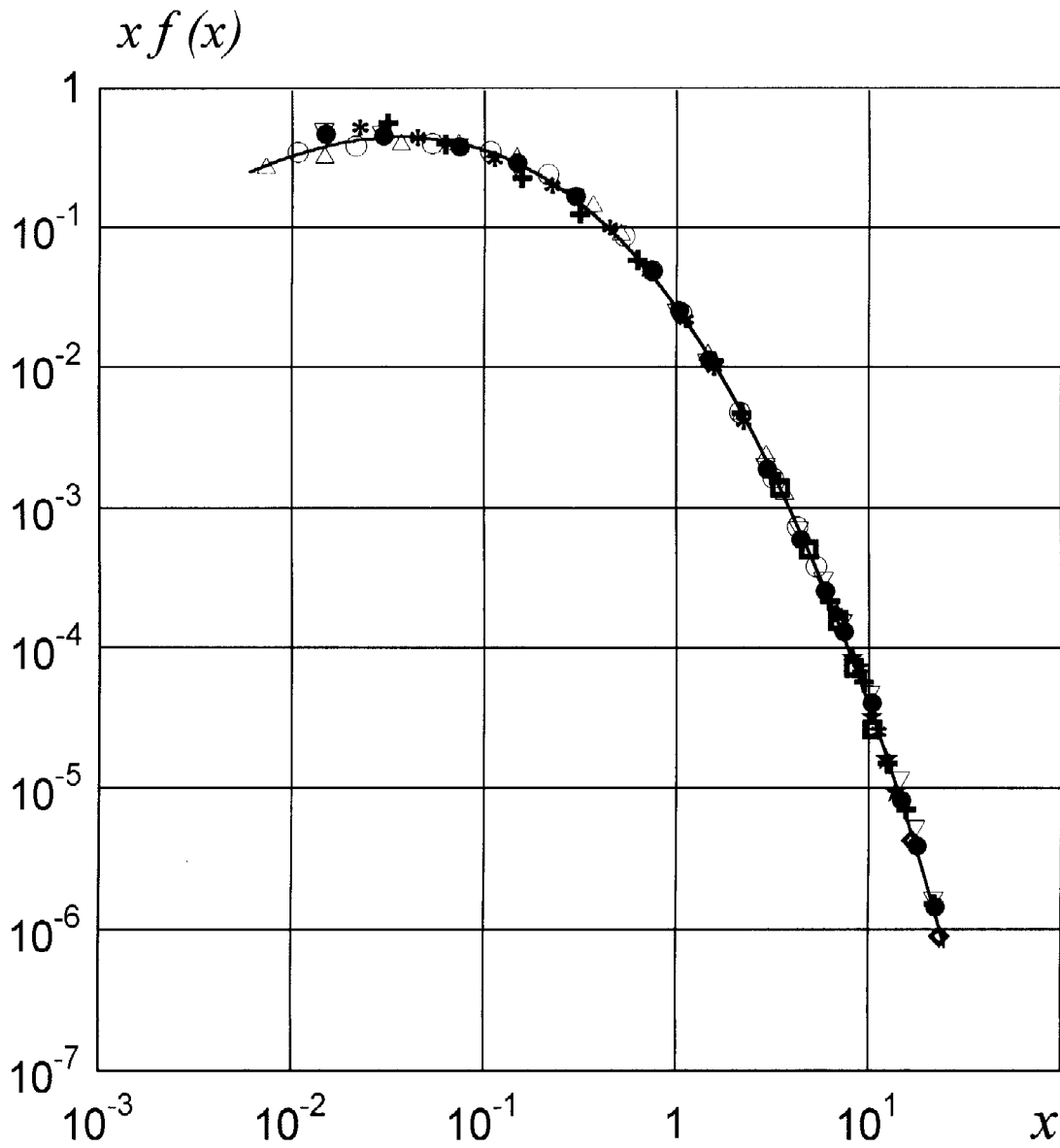
Figure 2. The dependence of the invariant part of the LDF of electrons on the scaling variable $x = r/r_{\text{m.s.r.}}(E, s)$.

$\diamond - E_\gamma = 10^2$ GeV, $s = 0.6$; $+ - E_\gamma = 10^5$ GeV, $s = 0.6$;

$* - E_\gamma = 10^4$ GeV, $s = 0.8$; $\bullet - E_\gamma = 10^5$ GeV, $s = 1.0$;

$\nabla - E_\gamma = 10^9$ GeV, $s = 1.0$; $\circ - E_\gamma = 10^4$ GeV, $s = 1.2$;

$\triangle - E_\gamma = 10^4$ GeV, $s = 1.4$; $\square - E_\gamma = 10^5$ GeV, $s = 1.4$;

$\star - E_\gamma = 10^6$ GeV, $s = 1.4$.   The solid curve is from our fitting function (11).

Table 2

Correction factor $\gamma(t, E)$ [19]

t, rad. units	Primary photon energy, GeV						
	10	10^2	10^3	10^4	10^5	10^6	10^7
1	1.02	1.01	1.06	1.14	1.24	1.35	1.47
2	1.06	1.04	1.07	1.13	1.22	1.32	1.45
4	1.09	1.06	1.05	1.06	1.12	1.19	1.28
6	1.10	1.06	1.03	1.02	1.07	1.11	1.16
8	1.15	1.08	1.04	1.01	1.05	1.06	1.09
10	1.20	1.11	1.05	1.01	1.04	1.02	1.06
12	1.36	1.18	1.09	1.03	1.05	1.04	1.04
14	1.56	1.28	1.15	1.07	1.06	1.05	1.04
16	1.76	1.39	1.21	1.11	1.09	1.07	1.04
18	2.06	1.52	1.29	1.19	1.13	1.09	1.06
20	2.40	1.70	1.41	1.25	1.18	1.12	1.09
22	2.81	1.92	1.56	1.33	1.24	1.17	1.11
24	3.32	2.22	1.72	1.44	1.30	1.22	1.16
26	3.93	2.54	1.91	1.57	1.38	1.28	1.21
28	4.65	2.92	2.14	1.72	1.48	1.35	1.26

of the adjoint equations were described in the following way:

$$N(t, E) = \gamma(t, E) N_G(t, E).$$

Here $N_G(t, E)$ is the value given by the well known Greisen's formula

$$N_G(t, E) = \frac{0.31}{\sqrt{\ln(E/\beta)}} \exp\{(1 - \frac{3}{2} \ln s')t\},$$

$$s = \frac{3t}{t + 2\ln(E/\beta)}.$$

The correction factor $\gamma(t, E)$ presented in Table 2 ($t_0 = 36.1$ g/cm^2, $\beta = 80$ MeV) gives information about accuracy of Greisen's formula in the high energy region.

The case of the real atmosphere

The analysis of our calculational results [7,8,12] shows that in the depth region $s \leq 1.0$ the lateral distribution practically coincides with the same distribution function for the homogeneous atmosphere with a density equal to the real atmosphere density at the observation level. In the post-maximum region ($s \geq 1$) the distribution function for the real atmosphere has a width some greater than that for the homogeneous one. The most significant difference belween them is found in the range of the distances $r \geq 10^2$ m from the shower axis (it can exceed over $(20 \div 30)\%$). The influence of the altitude density variation on the lateral distribution may be described by introducing into $f(r, E, s)$ for

homogeneous atmosphere the scale factor η:

$$\eta(E, s, t_{\text{obs}}) = \frac{\rho_{obs}}{\rho_0} \cdot \frac{r_{\text{m.s.r.}}^{\text{inhom}}}{r_{\text{m.s.r.}}}.$$

The following approximate expression takes place:

$$f^{\text{inhom}}(r, E, s, t_{\text{obs}}) = \left(\frac{\rho_{\text{obs}}}{\eta\rho_0}\right)^2 f\left(\frac{r\rho_{\text{obs}}}{\eta\rho_0}, E, s\right). \tag{12}$$

Here ρ_{obs} is the density of the real atmosphere at the observation level, $\rho_0 = 1.22 \cdot 10^{-3}$ g/cm^3. The values of η are presented in Table 3.

Figure 3–6 show the electron lateral distribution in the real atmosphere at 850 g/cm^2. It is seen that the results of Monte Carlo simulations are in a good agreement with LDF obtained from (12) by means of the transformation $f(x) \to f(r) \to f^{\text{inhom}}(r)$.
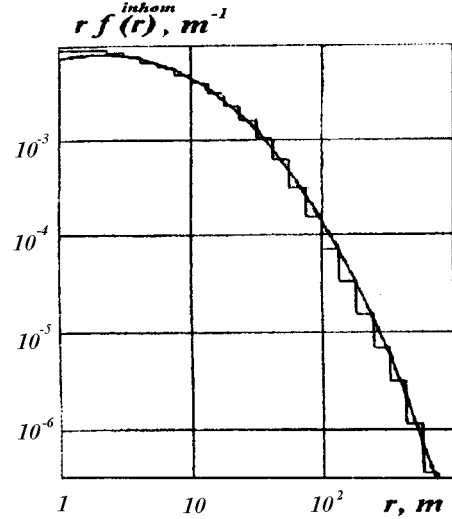
Figure 3. The electron lateral distribution in the real atmosphere at 850g/cm^2. $E = 10^6$ GeV, $s = 0.8$. ⌐⌐ — Monte Carlo simulations; — — data obtained from (12).

3. The lateral distribution of the electrons in the extensive air shower

The Monte-Carlo calculations are performed for the primary proton energies $E_p = (10^5 \div 10^9)$ GeV, the different observation levels $t_{obs} = (20.0 \div 28.5)$ c.u. and the radial distances from shower axis $r = (10 \div 3000)$ m.
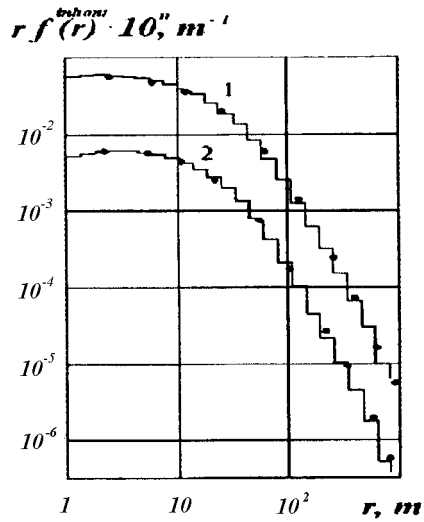
Figure 4. The electron lateral distribution in the real atmosphere at 850 g/cm^2. ¬⌐ — Monte Carlo simulations; • — data obtained from (12). 1 — $E = 10^5$ GeV(n=1); 2 — $E = 10^2$ GeV(n=0). $s = 1.0$

Figure 6. The electron lateral distribution in the real atmosphere at 850 g/cm^2. $E = 10^5$ GeV, $s = 1.4$. ¬⌐ — Monte Carlo simulations; —— — data obtained from (12).

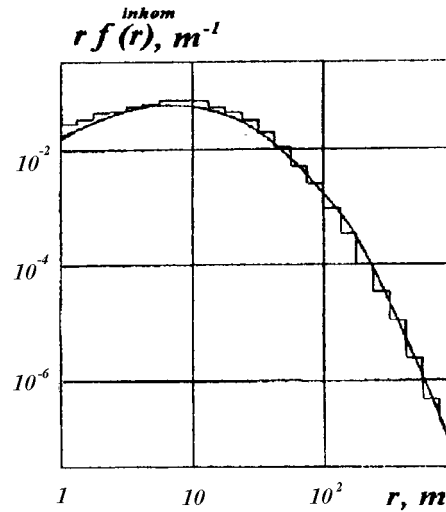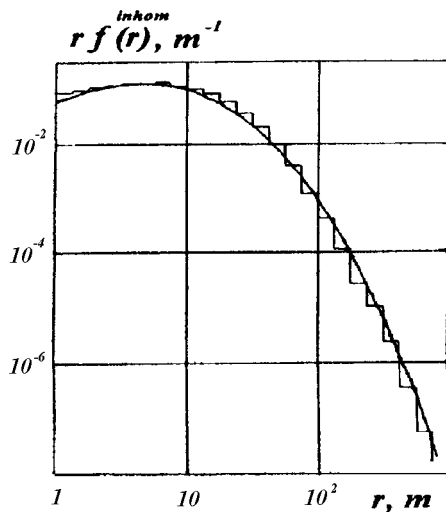Figure 5. The electron lateral distribution in the real atmosphere at 850 g/cm^2. $E = 10^5$ GeV, $s = 1.2$. ¬⌐ — Monte Carlo simulations; —— — data obtained from (12).

Table 3

The values of the scale factor $\eta(E, s, t_{\mathrm{obs}})$ [7]

t_{obs}, c.u.	E_γ GeV	s					
		0.6	0.8	1.0	1.2	1.4	1.6
28.5	10^2	1.00	1.01	1.02	1.04	1.07	1.10
	10^3	1.00	1.02	1.03	1.05	1.08	1.12
	10^5	1.00	1.02	1.04	1.06	1.10	-
	10^7	1.00	1.02	1.04	1.07	-	-
25.5	10^2	1.01	1.02	1.04	1.05	1.08	1.12
	10^3	1.02	1.03	1.04	1.06	1.10	1.15
	10^5	1.02	1.03	1.05	1.08	1.12	-
	10^7	1.02	1.04	1.06	1.09	-	-
23.0	10^2	1.01	1.02	1.04	1.06	1.09	1.13
	10^3	1.02	1.03	1.04	1.07	1.11	1.16
	10^5	1.02	1.03	1.06	1.09	-	-
	10^7	1.02	1.04	1.06	-	-	-
20.0	10^2	1.02	1.03	1.05	1.07	1.10	1.14
	10^3	1.02	1.04	1.06	1.08	1.11	-
	10^5	1.03	1.04	1.07	1.10	-	-
	10^7	1.03	1.05	1.07	-	-	-

The event generator

The event generator is based on the quark-gluon string model [20–23] with the use of algorithm [24,25]. According to this algorithm, in each elementary act the simulation starts from the calculations of energy fractions carried by leading barions, charged and neutral secondary hadrons, that allows to reproduce not only mean values, but also the fluctuations of total and partial inelasticity coefficients, multiplicities and the energy spectra of produced hadrons.

For the spectra of secondary hadrons and the cross sections of $hA-$interactions we used the results of quark-qluon string model [22] (see Fig. 7). The total cross section of $p - air$ interactions is aproximated by the formula [19] (see Fig. 8).

$$\sigma_{p-air}(E) = 273[1 + 0,068\ln(E/10^3 \ GeV)] \ mb. \tag{13}$$

As a result we have got the basic characteristics of interactions, being in the good agreement with experimental data and with the number of other well known numerical generators (see tab. 4,5).

The method of estimation of lateral distribution function

To describe the LDF of electrons in the pure electromagnetic cascade we resort to the scaling parametrization given in the sections 2–3.

Using the formulas mentioned above we have estimated the total number of electrons in EAS at the observation level $N_p(E_p, t_{obs})$, the mean square radius of the shower $R_{m.s.r.}(E_p, t_{obs})$ and the lateral distribution function $F(r, E_p, t_{obs})$. Here and further on the capital symbols $R_{m.s.r.}$ and F designate the characteristics of EAS in opposition to the corresponding lower case symbols used for the EMC characteristics (see Eq. (7), (9)).

Results

Our results on the average electron number at observation level and the average depth of maximum with the comparison with the data from other well known models presented in tables 6,7.

The comparison of our calculation results with the data obtained in the framework of the quark-gluon string model [19] on the cascade curves and the lateral distribution of electrons for proton induced showers is presented in Fig. 9,10.

Similarly to the electromagnetic cascade case, for the analysis of the lateral distribution of electrons in EAS we use the scaling variable $X = r/R_{m.s.r.}$.

We have found out that the LDF in the radial region $X \geq 0.05$ is well described by the formula

$$R_{m.s.r.}(E_p, t_{obs}) \, r \, F(r, E_p, t_{obs}) = X \, F(X),$$

i.e. it demonstrates the same type of scaling as the LDF in pure electromagnetic cascade (see Eq. (8), (10)). The dependence of the invariant part $X \, F(X)$ on the scaling variable X is shown on Fig. 11.

Besides the scaling function $X \, F(X)$ does not practically differ from the one given by Eq. (11) for the case of pure electromagnetic cascade.

It seems to be very important to investigate the sensitivity of this scaling property to the variation of basic parameters of the hadron-nucleous interactions model. We have made calculations for various values of parameters of model determining the average energy fractions carried by secondary hadrons in p-Air collisions and obtained the same result. It means that if we use the scaling vaiable $X = r/R_{m.s.r.}(E_p, t_{obs})$ then almost all influence of hadron-nucleous interactions model on the radial distribution in EAS is realized through the only one characteristic — the mean square radius of shower.

Conclusions

In this paper we report on the results obtained for the lateral distribution of the electrons in the electromagnetic cascade and in the extensive air shower in the radial distance range $r = (10 \div 3000)$ m. The Monte Carlo simulations of EAS were perfomed using the model of quark-qluon strings for the hadron-nucleous interactions. We also used the new scaling parametrization of the lateral distribution function of charged particles in the pure electromagnetic cascade up to 3000 m.

We have found the new scaling property of the lateral distribution function in EAS generated by $10^5 \div 10^9$ GeV protons in the inhomogeneous atmosphere at the different observation levels. The LDF in the shower contains the same invariant part $F(X) = R^2_{m.s.r.} \, F(r, E_p, t_{obs})$ as the lateral distribution in pure electromagnetic cascade shower.

It is important to note that the scaling function $X \, F(X)$ does not practically differ from $x \, f(x)$ given by Eq. (11) for the EMC. This fact proves the validity of the lateral distribution function in pure electromagnetic cascade for the description of LDF in the extensive air shower.

It is also significant that the form of the scaling function is very poorly sensitive to the change of energy ballance between the shower components.

The results presented in this paper allow to solve some problems appearing in the design studies of
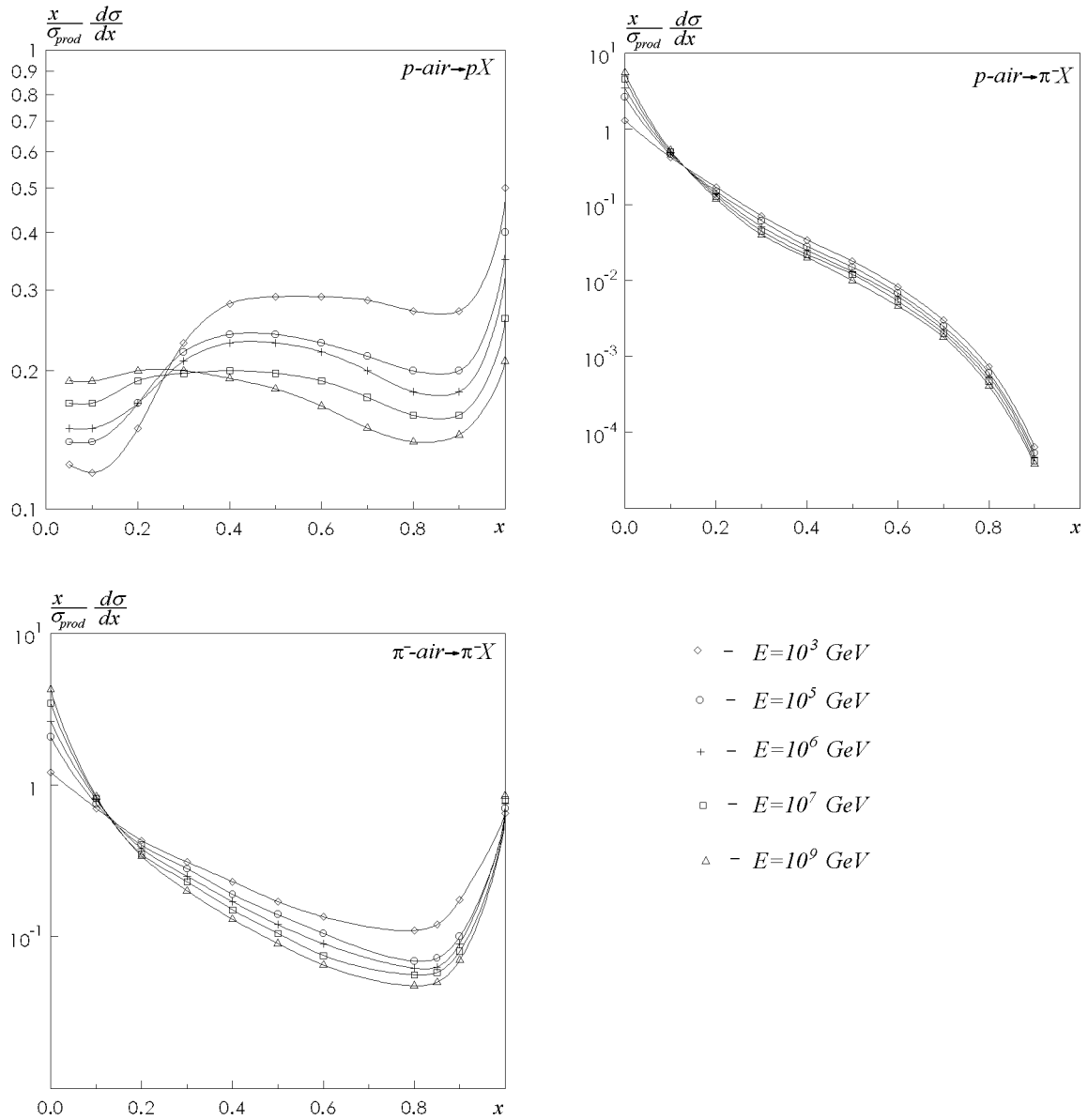
Figure 7. The spectra of secondary p and π^- produced in $p - air$ and $\pi^- - air$ collisions [22] used in our calculations
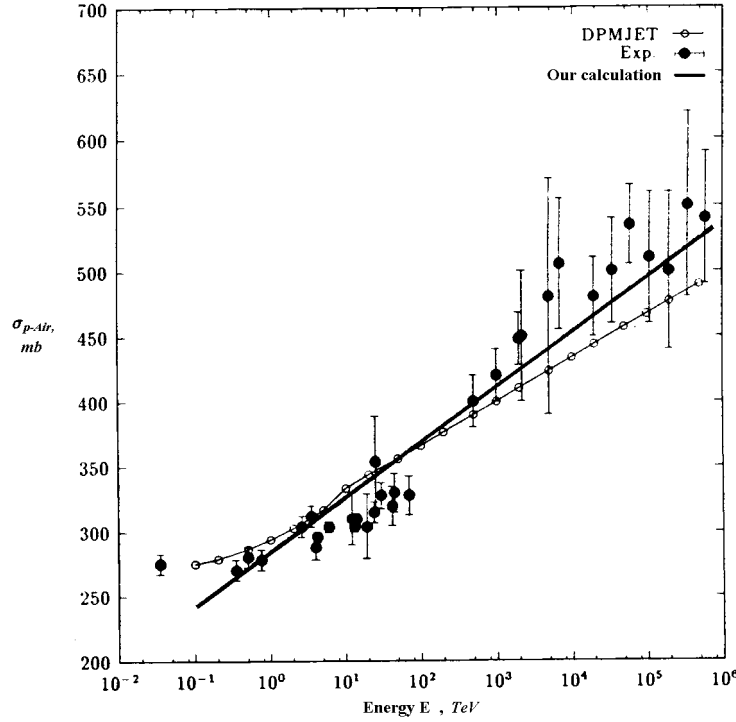
Figure 8. The total cross section σ_{p-air} as function of the collision energy. The results of approximation (13) used in our calculations is compared to the calculation of the Glauber model in DPMGET-II [26] and cosmic ray data [28].

Table 4

Average elasticities of leading barions (K_{lh}) charged (K_{ch}) and neutral (K_0) secondary hadrons in p-air collisions. Comparison of our calculational results with the data obtained from DPMJET-II [26]

E,	K_{lh}		K_{ch}		K_0	
GeV	Our results	DPMGET-II	Our results	DPMGET-II	Our results	DPMGET-II
10^3	0.351	0.369	0.390	0.347	0.216	0.215
10^4	0.335	0.336	0.399	0.367	0.222	0.225
10^5	0.297	0.313	0.423	0.381	0.233	0.231
10^6	0.282	0.286	0.431	0.397	0.239	0.240
10^7	0.255	0.260	0.448	0.413	0.248	0.250
10^8	0.231	0.243	0.461	0.422	0.256	0.255

Table 5

Average atmospheric depths of first interaction and their standard deviations (in g/cm^2) for proton induced showers. Comparison of our calculational results with the data obtained from other well known event generators [27]

E, GeV	Our results	HDPM	VENUS	SIBYLL	QGSJET	DPMGET
10^5	78.1 ± 78.4	79.4 ± 83.8	77.3 ± 78.7	75.9 ± 77.2	80.3 ± 88.6	75.2 ± 75.4
10^6	70.9 ± 71.1	66.0 ± 66.7	71.1 ± 72.2	69.6 ± 68.6	73.6 ± 69.4	77.1 ± 82.5

42

Average electron numbers at observation level (100 m a.s.l.) for proton induced showers. Comparison of our calculational results with the data obtained from other well known event generators [27]

E, GeV	Our results	HDPM	VENUS	SIBYLL	QGSJET	DPMGET
10^5	7812	9644	7745	9541	8530	6851
10^6	131021	162209	131093	158902	136475	111533

Average depth of maximum (in g/cm^2) for proton induced showers. Comparison of our calculational results with the data obtained from other well known event generators [27]

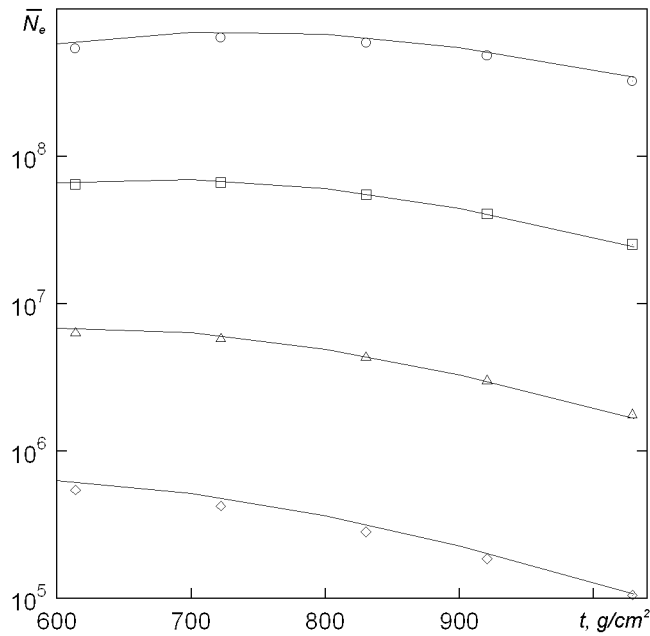| E, GeV	Our results	HDPM	VENUS	SIBYLL	QGSJET	DPMGET
10^5	503	521	503	519	504	492
10^6	580	599	574	592	576	560

Figure 9. The cascade curves of electrons for proton induced showers. Comparison of our calculational results (solid curves) with the data obtained in the framework of the quark-gluon string model [19]: $\circ - E_0 = 10^9$ GeV; $\square - E_0 = 10^8$ GeV; $\triangle - E_0 = 10^7$ GeV; $\diamond - E_0 = 10^6$ GeV.
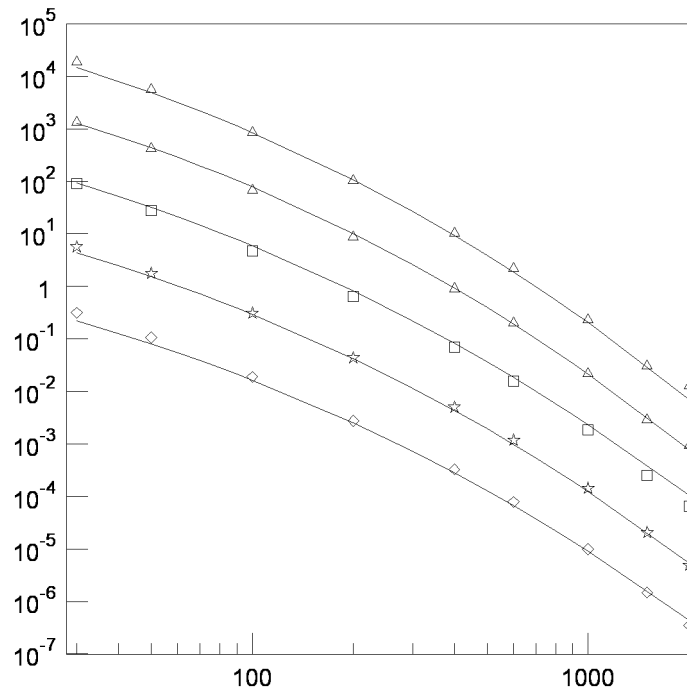
43

Figure 10. The lateral distribution of electrons for proton induced showers. Comparison of our calculational results (solid curves) with the data obtained in the framework of the quark-gluon string model [19]: $\circ - E_0 = 10^9$ GeV; $\square - E_0 = 10^8$ GeV; $\triangle - E_0 = 10^7$ GeV; $\diamond - E_0 = 10^6$ GeV; $\star - E_0 = 10^5$ GeV.

new large air shower arrays and the interpretation of the observational data connected with many debatable aspects in the field of hadronic interactions.
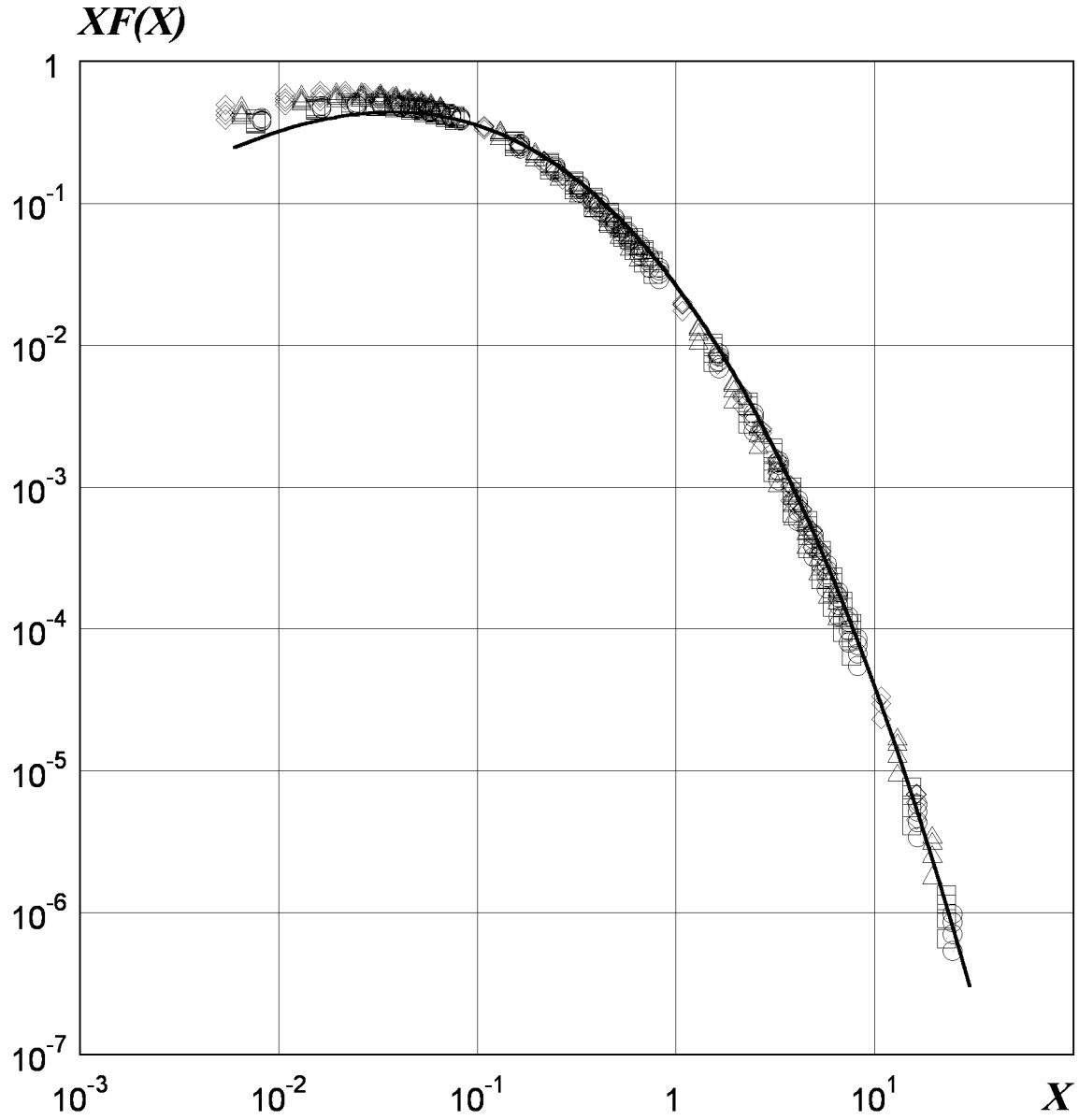
XF(X)

Figure 11. The dependence of the invariant part of the lateral distribution function of electrons in EAS on the scaling variable $X = r/R_{m.s.r.}(E_p, t_{obs})$.
$\diamond - E_0 = 10^5$ GeV $\square - E_0 = 10^8$ GeV   ———— - the fitting function given by Eq. (11)
$\triangle - E_0 = 10^7$ GeV $\bigcirc - E_0 = 10^9$ GeV $t_{obs}(c.u.) = 28.5;\ 25.5;\ 23.0;\ 20.0$

References

1. Nishimura J. // Handbuch der Physik., 1967, 46/2, p.1.

2. Allan H. R. et al. // Proc. of 14-th Inter. Cosmic Ray Conf., Munich, 1975, v.8, p.3071.

3. Dedenko L. G. et al. // Proc. of 14-th Inter. Cosmic Ray Conf., Munich, 1975, v.8, p.2731.

4. Dedenko L. G., Nikolsky S. I., Stamyenov I. N. // Kratk. soobsh. po fis., FIAN, 1976, v.1, p.30.

5. Hillas A., Lapikens J. // Proc. of 15-th Inter. Cosmic Ray Conf., Plovdiv, 1977, v.8, p.460.

6. Lagutin A. A., Plyasheshnikov A. V., Uchaikin V. V. // Proc. of 16-th Inter. Cosmic Ray Conf., Kyoto, 1979, v.7, p.18.

7. Plyasheshnikov A. V., Konopelko A. K., Vorobiev K. V. Preprint FIAN, Moscow, N 92, 1988.

8. Goncharov A. I. Ph. D. Thesis, Altai State University, 1991.

9. Goncharov A. I., Konopelko A. K., Lagutin A. A. et al. // Izv. AN SSSR. Ser. fiz., 1991, v.55, p.724.

10. Goncharov A. I., Lagutin A. A. // Proc. of 24-th Inter. Cosmic Ray Conf., Roma, 1995, v.1, p.213.

11. Lagutin A. A., Plyashshnikov A. V., Melentjeva V. V. Preprint of the Altai State University, Barnaul, N 96/2, 1996.

12. Lagutin A. A., Plyasheshnikov A. V., Goncharov A. I. Preprint of the Altai State University, Barnaul, N 97/1, 1997.

13. Lagutin A. A., Plyasheshnikov A. V., Goncharov A. I. // Nuclear Physics B (Proc. suppl.), 1997, 60 B, pp.161.

14. Plyasheshnikov A. V., Vorobiev K. V. // Proc. of 17-th Inter. Cosmic Ray Conf., Paris, 1981, v.5, p.206.

15. Konopelko A. K., Plyasheshnikov A. V. // Nuclear Physics B (Proc. Suppl.), 1997, 52 B, p.152.

16. Plyasheshnikov A. V., Lagutin A. A., Uchaikin V. V. // Proc. of 16-th Inter. Cosmic Ray Conf., Kyoto, 1979, v.7, p.1; p.13.

17. Hillas A. M. // Proc. of 17-th Inter. Cosmic Ray Conf., Paris, 1981, v.6, p.244.

18. Lagutin A. A., Plyasheshnikov A. V., Uchaikin V. V., // Proc. of 17-th Inter. Cosmic Ray Conf., Paris, 1981, v.5, p.194.

19. Lagutin A. A., Uchaikin V. V., Chernyaev G. V., Shabelski Yu.M. // Preprint LNPI (Leningrad), N 1289, 1987.

20. Kaidalov A. B., Ter-Martirosyan K. A. // Yad. Fiz., 1984, v.39, p.1545; v.40, p.211.

21. Kaidalov A. B., Ter-Martirosyan K. A., Shabelski Yu. M. // Yad. Fiz., 1986, v.43, p.1282.

22. Shabelski Yu. M. Preprint LNPI, Leningrad, N 1224, 1986.

23. Shabelski Yu. M. // Yad. Fiz., 1986, v.44, p.186;v.45, p.223.

24. Litvinov V. A. Ph. D. Thesis, Altai State University, 1986.

25. Uchaikin V. V., Ryzhov V. V. The stochastic theory of high energy particles transport (in Russian), Novosibirsk, 1988.

26. Battistoni G., Forti C., Ranft J. // Astroparticle Physics, 1995, v.3, p.157.

27. Knapp J., Heck D., Schatz G. // Forschungszentrum Karlsruhe, FZKA 1996, p.5828.

28. Mielke H. H., Föller M., Engler J. and Knapp J., // J. Phys G, 1994, v.20 p.637.